JUSTC

Article

http://justc.ustc.edu.cn

Received: November 03, 2025; Accepted: March 01, 2026

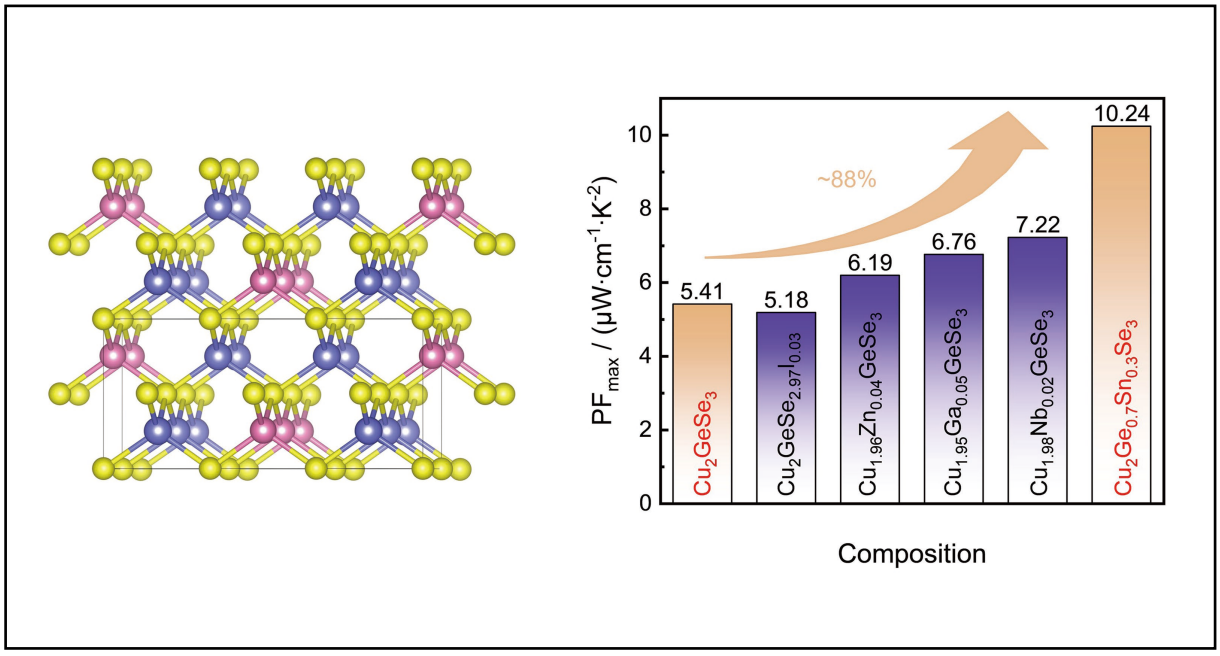
Synergistic Optimization of Mobility and Effective Mass by Sn Alloying Leads to Enhanced Thermoelectric Performance in Cu_2GeSe_3

Jiating Xia[1,2], Liang Sun[2], Wei Bai[2], Ni Ma[1,2] ✉, and Chong Xiao[2] ✉

[1]*State Key Laboratory of Precision and Intelligent Chemistry, School of Chemistry and Materials Science, University of Science and Technology of China, Hefei 230026, China;*
[2]*Hefei National Research Center for Physical Sciences at the Microscale, University of Science and Technology of China, Hefei 230026, China*

✉Correspondence: Ni Ma, E-mail: mani@ustc.edu.cn; Chong Xiao, E-mail: cxiao@ustc.edu.cn
© 2026 The Author(s). This is an open access article under the CC BY-NC-ND 4.0 license (http://creativecommons.org/licenses/by-nc-nd/4.0/).

Graphical abstract



Schematic diagram of the crystal structure of Cu_2GeSe_3 and the enhanced power factor of a series of samples

Public summary

- $Cu_2Ge_{1-x}Sn_xSe_3$ (x = 0–0.4) series samples were prepared by a high-temperature solid-state reaction followed by hot pressing.
- The incorporation of Sn effectively increases the formation energy of both Cu_{Ge} and V_{Cu} defects, thereby significantly enhancing the carrier mobility. Concurrently, the increased difference in electronegativity induced by Sn alloying leads to a larger effective mass (m*), which is responsible for the notable increase in the Seebeck coefficient. Consequently, these effects lead to a substantially enhanced power factor (PF), reaching 10.22 μW·cm^{-1}·K^{-2} at 723 K. This value represents an ~80% increase over that of pristine Cu_2GeSe_3.
- This work demonstrates that alloying is a highly effective strategy for enhancing the thermoelectric performance of copper-based materials.

Citation: Xia J T, Sun L, Bai W, et al. Synergistic Optimization of Mobility and Effective Mass by Sn Alloying Leads to Enhanced Thermoelectric Performance in Cu_2GeSe_3. *JUSTC*, **2026**, 56(6): . CSTR: 32290.14.JUSTC-2025-0118. DOI: 10.52396/JUSTC-2025-0118

JUSTC

Article

http://justc.ustc.edu.cn

Received: November 03, 2025; Accepted: March 01, 2026

Synergistic Optimization of Mobility and Effective Mass by Sn Alloying Leads to Enhanced Thermoelectric Performance in Cu_2GeSe_3

Jiating Xia[1,2], Liang Sun[2], Wei Bai[2], Ni Ma[1,2] ✉, and Chong Xiao[2] ✉

[1]*State Key Laboratory of Precision and Intelligent Chemistry, School of Chemistry and Materials Science, University of Science and Technology of China, Hefei 230026, China;*

[2]*Hefei National Research Center for Physical Sciences at the Microscale, University of Science and Technology of China, Hefei 230026, China*

✉Correspondence: Ni Ma, E-mail: mani@ustc.edu.cn; Chong Xiao, E-mail: cxiao@ustc.edu.cn

© 2026 The Author(s). This is an open access article under the CC BY-NC-ND 4.0 license (http://creativecommons.org/licenses/by-nc-nd/4.0/).

Cite This: *JUSTC*, **2026**, 56(6): (8pp)

Read Online

SI Supporting Information

Abstract: Cu-based materials, renowned for their environmentally friendly characteristics, have become highly promising candidates for thermoelectric applications because of their excellent thermoelectric properties. However, their intrinsically low carrier mobility restricts further enhancement of thermoelectric performance. In this work, Sn alloying not only enhanced the carrier mobility of Cu_2GeSe_3 but also increased its effective mass, leading to markedly improved thermoelectric properties. The incorporation of Sn effectively increases the formation energy of Cu_{Ge} defects and V_{Cu} vacancies, thereby substantially increasing carrier mobility. Moreover, the greater difference in electronegativity of the Sn-alloyed material results in an increased effective mass (m^*), which contributes to a remarkable improvement in the Seebeck coefficient. Consequently, these two effects result in a notable increase in PF, reaching 10.22 $\mu W \cdot cm^{-1} \cdot K^{-2}$ at 723 K, representing an increase of approximately 80% compared with that of pristine Cu_2GeSe_3. Additionally, Sn alloying introduces point defect scattering that further decreases the lattice thermal conductivity (κ_{lat}). Combined with the enhanced power factor (PF), this reduction yields a maximum ZT of ~0.66 at 723 K. Our findings highlight Sn alloying as an effective approach for enhancing thermoelectric performance, providing a rational pathway for developing high-performance copper-based thermoelectric materials.

Keywords: Thermoelectric material; Sn alloying; Carrier mobility; Cu_2GeSe_3

CLC number: TB34 **Document code:** A

1 Introduction

Thermoelectric materials, which are capable of directly converting thermal energy into electrical energy, offer distinct advantages, such as being noiseless, pollution-free, safe and reliable. These characteristics make them highly promising for sustainable development initiatives[1–2]. The conversion efficiency is related to the dimensionless figure of merit, $ZT = S^2\sigma T/(\kappa_{ele} + \kappa_{lat})$, where S is the Seebeck coefficient, σ is the electrical conductivity, T is the absolute temperature, κ_{ele} is the electronic thermal conductivity, and κ_{lat} is the lattice thermal conductivity[3–5]. High σ, large S, and low κ_{lat} are crucial characteristics of an ideal thermoelectric material. However, the strong interdependence of these parameters severely limits the enhancement of thermoelectric performance. Overcoming this challenge requires a fundamental understanding of the material's physical properties. This deeper insight has facilitated advanced optimization strategies, which focus primarily on enhancing electrical properties through valence band convergence, band flattening, and resonant doping[6–10] and reducing κ_{lat} by introducing lattice defects, utilizing lone pair electrons, and exploiting liquid-like cationic motion[11–13].

Copper-based compounds such as Cu_2Se, $CuGaTe_2$, CuAgSe, and BiCuSeO have attracted significant interest because of their excellent thermoelectric performance[13–16]. Among them, Cu_2SnSe_3 is a P-type semiconductor in which Cu–Se bonds dominate hole transport, while Sn atoms donate electrons and scatter phonons[17,18]. This unique property, which conforms to the "phonon-glass-electron-crystal" (PGEC) concept[19], makes this compound a promising candidate for thermoelectric application. Cu_2GeSe_3, analogous to Cu_2SnSe_3, has also been hypothesized to exhibit PGEC characteristics[18,20–23]. However, its relatively low mobility restricts further improvement of its thermoelectric properties. Since defects typically have a significant effect on carrier mobility and given that considerable research has been devoted to defects in Cu-based compounds[24–27], understanding the charge transport mechanisms in diamond-like Cu_2GeSe_3 is crucial. This study therefore focuses on enhancing the thermoelectric performance of Cu_2GeSe_3 through the manipulation of its intrinsic lattice defects.

In this work, we prepared a $Cu_2Ge_{1-x}Sn_xSe_3$ solid solution and achieved a peak PF of ~10.22 $\mu W \cdot cm^{-1} \cdot K^{-2}$ at 723 K, which is higher than the values reported in previous

CSTR: 32290.14.JUSTC-2025-0118
DOI: 10.52396/JUSTC-2025-0118
JUSTC, **2026**, 56(6):

studies[20,22]. Improvements in the mobility and Seebeck coefficient significantly increase the PF of the sample. Additionally, the solid solution effectively reduces κ_{lat} because of the enhanced phonon scattering by point defects. The concurrent optimization of electrical and thermal properties resulted in a marked increase in the *ZT*. Compared with that of the pristine material, the *ZT* value of the $Cu_2Ge_{0.7}Sn_{0.3}Se_3$ sample increased significantly from 0.28 to 0.66 at 723 K, highlighting its exceptional performance.

2 Materials and methods

2.1 Synthesis

The samples were prepared using the following reagents: Cu powder (99.9%, Aladdin), Ge powder (99.99%, Aladdin), Sn powder (99.99%, Aladdin), and Se powder (99.99%, Aladdin). The elements were loaded into a silica tube according to the stoichiometric ratio. The evacuated silica tubes were heated to 1203 K and held at this temperature for 48 h. Then, the ingots were ground into a fine powder, and the obtained powders were sintered in a graphite die by hot pressing at 903 K under 70 MPa for 30 min.

2.2 Phase and microstructural characterization

Powder X-ray diffraction (PXRD) patterns were obtained on a Rigaku TTR-III powder X-ray diffractometer (Cu Kα radiation λ = 1.5406 Å) in the 2θ range from 10° to 70° with a step of 0.02°. Semiquantitative elemental analysis was performed on a scanning electron microscope (SEM) (HITACHI SU-8220) equipped with an energy dispersive spectroscope (EDS). High-angle annular dark-field scanning transmission electron microscopy (HAADF-STEM) images were obtained on a JEM-ARM200F. The room-temperature solid-state ultraviolet–visible spectroscopy (UV–vis) spectra were measured using a Shimadzu SOLID 3700 DUV spectrometer. X-ray photoelectron spectroscopy (XPS) measurements were performed using a Thermo Scientific ESCALAB 250Xi spectrometer.

2.3 Thermoelectric property measurements

A Cryoall CTA-3 instrument system in a He atmosphere was used to measure the Seebeck coefficient and electrical conductivity from room temperature to 723 K. The total thermal conductivity (κ_{tot}) was obtained from the equation $\kappa_{tot} = D \times C_p \times \rho$, where the thermal diffusivity (*D*) was measured using the laser flash diffusivity method on a NETZSCH LFA–467 in a N_2 atmosphere, the heat capacity (C_p) was estimated by Dulong-Petit law, and the density (ρ) was determined from the dimensions and mass of the samples after hot pressing. Hall measurements from room temperature to 673 K were performed on a Lake Shore 8400 series. The longitudinal (v_l) and transverse (v_t) sound velocities were measured by an ultrasonic measuring system at room temperature.

2.4 Defect formation energy calculation

The formation energy of a charged point defect can be expressed by the following formula:

$$E^q_{form} = E^q_{tot}(defect) - E^q_{tot}(perfect) - \sum_a n_a\mu_a + q_i(E_F + E_V + \Delta V)$$

where *Eq tot* (*defect*) and *Eq tot* (*perfect*) are the total energy of the perfect crystal and the compound with defects, respectively; n_a is the number of defects; μ_a is the chemical potential of element a; q_i is the charge of defects; E_F is the Fermi level relative to the valence band maximum E_V (VBM) of the perfect crystal; and ΔV is an electrostatic potential correction due to the finite-size effect between the defective and perfect system[1,2]. Energy calculations were performed by the Vienna ab initio simulation package (VASP) based on density functional theory (DFT)[28]. The generalized gradient approximation of Perdew–Burke–Ernzerhof (GGA-PBE) was applied as the exchange-correlation functional, and the cutoff energy of the plane wave was set as 500 eV[29,30].

3 Results and discussion

The PXRD patterns of the $Cu_2Ge_{1-x}Sn_xSe_3$ series (x = 0–0.4) are shown in Fig. 1a. The diffraction peaks of all the obtained samples were well indexed to the orthorhombic structure of Cu_2GeSe_3 (PDF # 04-016-2386, *Imm*2 space group). The Sn content was limited to x = 0.4 to prevent the formation of secondary phases. For comparison, the PXRD pattern of pristine Cu_2SnSe_3 (PDF # 04-012-4693, *Cc* space group) was also measured and is shown in Fig. S1 (see Supporting

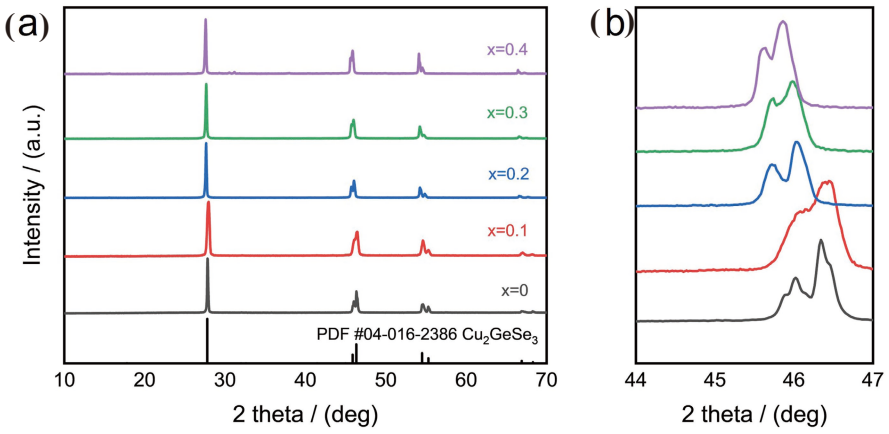


Fig. 1. XRD patterns of the $Cu_2Ge_{1-x}Sn_xSe_3$ ($0 \leqslant x \leqslant 0.4$) samples (a) and the amplification diffraction peak at 2θ angles of 44–47° (b).

CSTR: 32290.14.JUSTC-2025-0118
DOI: 10.52396/JUSTC-2025-0118
JUSTC, **2026**, 56(6):

information). An expanded view of the patterns in the 2θ range of 44–47° is shown in Fig. 1b, revealing a systematic peak shift toward lower angles with increasing Sn content. The observed shift is attributed to lattice expansion resulting from the isovalent substitution of the smaller Ge^{4+} ion (0.39 Å) with the larger Sn^{4+} ion (0.55 Å), leading to an increase in the unit cell parameters. To characterize the chemical environment, we performed XPS analysis (Fig. S2), and the Cu 2p spectrum exhibited spin–orbit split peaks at 952.3 eV ($2p_{1/2}$) and 932.5 eV ($2p_{3/2}$), corroborating the oxidation state of Cu^{+}. The Ge 2p peak observed at 1221.0 eV is characteristic of Ge^{4+}. Similarly, the peak located at 486.4 eV is characteristic of Sn^{4+}. The Se 3d spectrum reveals two components at 54.4 eV ($3d_{5/2}$) and 55.2 eV ($3d_{3/2}$), confirming the Se^{2-} state. XPS analysis confirms the chemical valences of Cu, Ge, Sn, and Se of +1, +4, +4, and −2, respectively, which is consistent with previous studies[20]. UV–Vis spectroscopy was used to determine the optical band gap of the material. The absorption data indicated a band gap of approximately 0.7 eV (Fig. S3), which is consistent with the literature value[31]. The band gaps of the two compounds remain almost unchanged.

The Cu_2GeSe_3 compound has a diamond-like structure, as illustrated in Fig. 2a. The corner-sharing $CuSe_4$ and $GeSe_4$ tetrahedral units, which constitute a monolayer structure corresponding to the yellow-highlighted region in Fig. 2a, are shown in Fig. 2b. A HAADF-STEM image of the Cu_2GeSe_3 sample along the [1 0 0] zone axis is shown in Fig. 2c, which is consistent with the lattice structure. The lattice size obtained from the HAADF image is shown in Fig. 2c. The crystal plane distance obtained from the HAADF images (0.57 nm) is in good agreement with the c-axis size (0.55 nm) in the crystal structure. These results confirm the successful synthesis of pure materials. Corresponding high-resolution EDS elemental maps for copper (Cu), germanium (Ge), and selenium (Se) are shown in Fig. 2d, revealing a uniform spatial distribution that matches the crystal structure. To examine the microstructure and morphology, scanning electron microscopy (SEM) was performed on hot-pressed samples, and the results are displayed in Fig. S4. Furthermore, EDS analysis was employed to determine the elemental distribution and composition. As summarized in Table S1 (see Supporting information), the elements were homogeneously distributed, and no secondary phases were detected in the bulk samples. These results collectively confirm the successful synthesis of both pristine and Sn-alloyed Cu_2GeSe_3 compounds.

The temperature-dependent electrical and thermal transport properties of the $Cu_2Ge_{1-x}Sn_xSe_3$ (x = 0–0.4) samples are shown in Fig. 3. All the samples exhibit degenerate semiconductor behavior, as evidenced by decreasing electrical conductivity with increasing temperature (Fig. 3a). Sn alloying

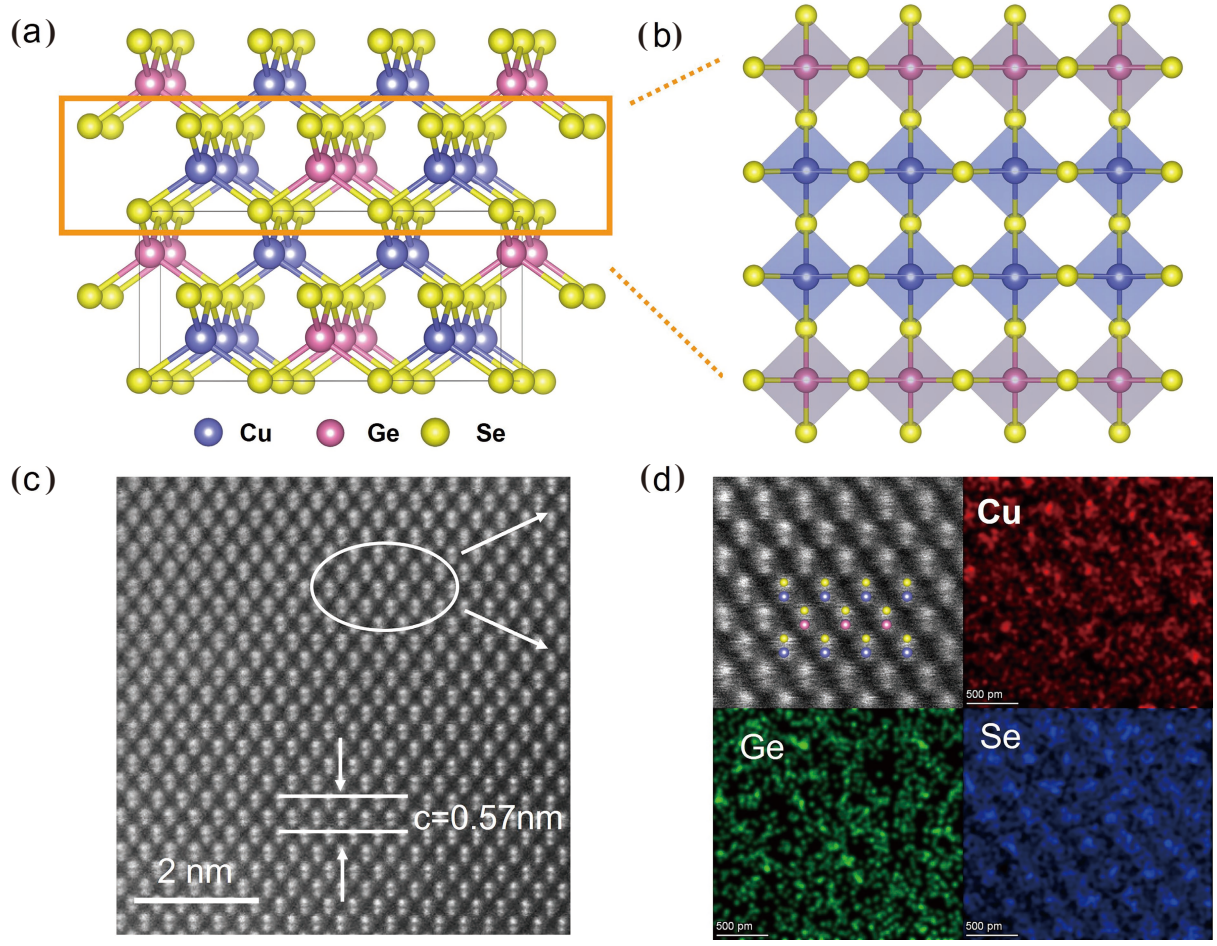


Fig. 2. (a) Crystal structure of Cu_2GeSe_3; (b) top view of the structure depicted in the orange region. (c) HAADF image along the [1 0 0] zone axes and (d) the corresponding EDS elemental intensity maps.

CSTR: 32290.14.JUSTC-2025-0118
DOI: 10.52396/JUSTC-2025-0118
JUSTC, **2026**, 56(6):

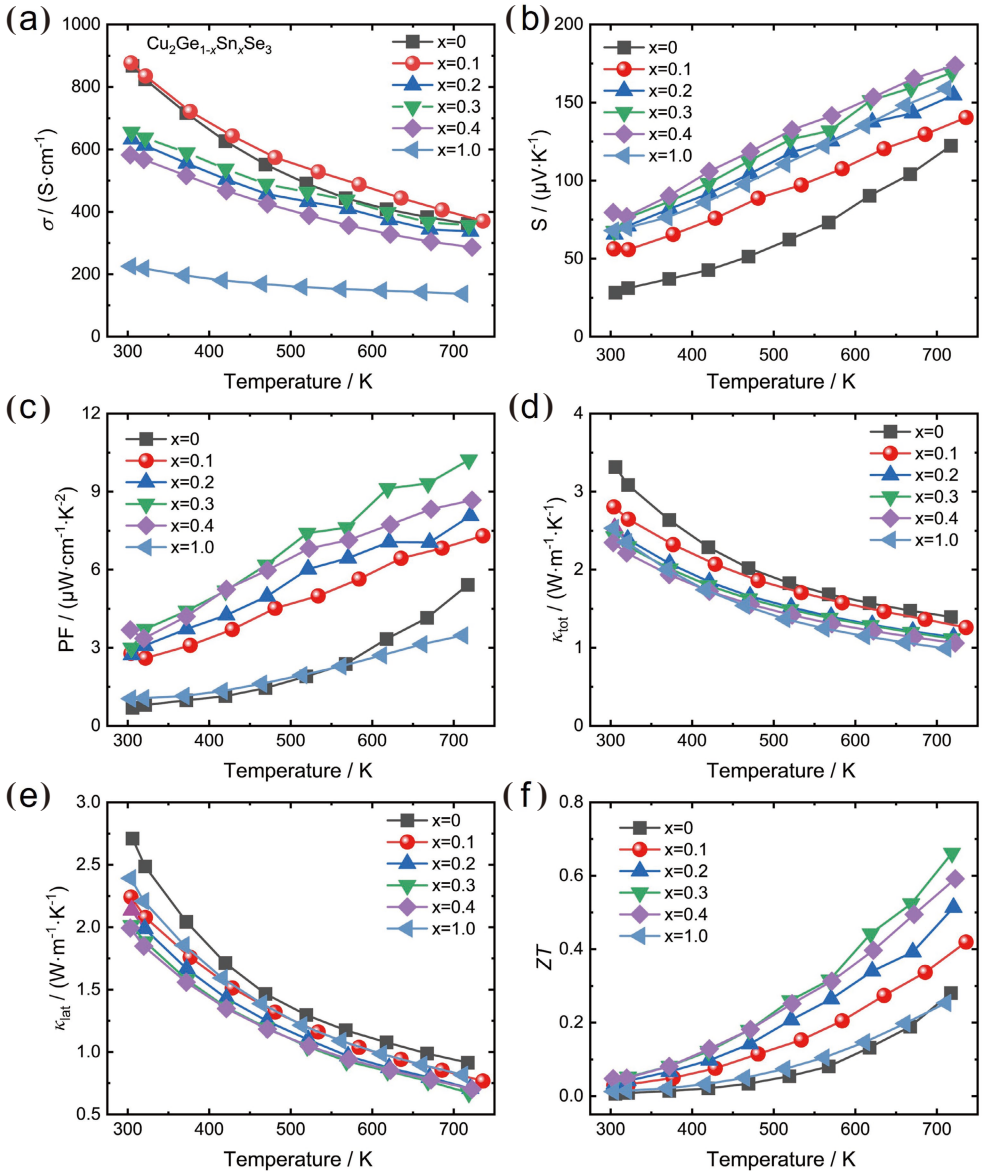


Fig. 3. Temperature-dependent (a) electrical conductivity, (b) Seebeck coefficient, (c) power factor, (d) total thermal conductivity, (e) lattice thermal conductivity and (f) *ZT* of $Cu_2Ge_{1-x}Sn_xSe_3$ ($0 \leqslant x \leqslant 0.4$) samples

progressively reduces the electrical conductivity from 867.87 $S \cdot cm^{-1}$ (pristine Cu_2GeSe_3) to 582.34 $S \cdot cm^{-1}$ ($Cu_2Ge_{0.6}Sn_{0.4}Se_3$), primarily because of the decreased carrier concentration. The reduction in the carrier concentration yields conductivities for all the solid solutions that fall within the bounds defined by the pristine compounds Cu_2GeSe_3 and Cu_2SnSe_3. The positive Seebeck coefficient of all the samples in Fig. 3b indicates p-type conduction. Moreover, the Seebeck coefficient is positively correlated with temperature, which is consistent with the observed changes in electrical conductivity. Remarkably, Sn alloying enhances the Seebeck coefficient by 177% (from 28.17 $\mu V \cdot K^{-1}$ in pristine Cu_2GeSe_3 to 78.14 $\mu V \cdot K^{-1}$ in $Cu_2Ge_{0.7}Sn_{0.3}Se_3$). The substantial increase in the Seebeck coefficient leads to a significant improvement in the PF of the solid solution samples, as evidenced in Fig. 3c. Among all the alloyed samples, the $Cu_2Ge_{0.7}Sn_{0.3}Se_3$ sample achieves a peak PF of ~10.22 $\mu W \cdot cm^{-1} \cdot K^{-2}$ at 723 K, which is 80% higher than that of the pristine Cu_2GeSe_3 and surpasses the previously reported $Cu_2GeSe_{2.96}S_{0.04}$ (~8.24 $\mu W \cdot cm^{-1} \cdot K^{-2}$) and $Cu_{1.9}Ag_{0.1}Ge_{0.997}Ga_{0.003}Se_3$ samples (~7.30 $\mu W \cdot cm^{-1} \cdot K^{-2}$)[20,22]. The better electrical transport performance of $Cu_2Ge_{0.7}Sn_{0.3}Se_3$ is a key characteristic of an excellent thermoelectric material. In addition to electrical properties, the thermal properties of a material critically influence its thermoelectric performance. Similarly, the variations in κ_{tot} and κ_{lat} with temperature for $Cu_2Ge_{1-x}Sn_xSe_3$ (x = 0–0.4) compounds are plotted in Fig. 3d and e. The room temperature κ_{tot} of the pristine sample decreases from 3.32 $W \cdot m^{-1} \cdot K^{-1}$ to 2.31 $W \cdot m^{-1} \cdot K^{-1}$ after Sn alloying into the Cu_2GeSe_3 compound. The reduction in κ_{tot} is attributed to two primary factors: a decrease in electrical conductivity, which directly influences the electronic component of thermal conductivity, and a pronounced increase in point defect scattering, which significantly decreases κ_{lat}. The κ_{ele} can be calculated from the Wiedemann–Franz relation from $\kappa_{ele} = L\sigma T$, where L is the

CSTR: 32290.14.JUSTC-2025-0118
DOI: 10.52396/JUSTC-2025-0118
JUSTC, **2026**, 56(6):

Lorenz number and is extracted as follows[32]:

$$L = \left[1.5 + exp\left(-\frac{|S|}{116}\right)\right] \times 10^{-8} \quad (1)$$

Then, κ_{lat} of the sample is obtained by directly subtracting κ_{ele} from κ_{tot}. A 20% reduction in κ_{lat} from 2.71 $W \cdot m^{-1} \cdot K^{-1}$ to 2.14 $W \cdot m^{-1} \cdot K^{-1}$ caused by Sn alloying at room temperature is shown in Fig. 3e. Consequently, the concurrent optimization of electrical and thermal properties enables significantly enhanced *ZT* values across all temperatures in Sn-alloyed samples (Fig. 3f). The maximum *ZT* improvement occurs in $Cu_2Ge_{0.7}Sn_{0.3}Se_3$, where the peak value increases from ~0.28 to ~0.66 at 723 K, which is a 2.4-fold increase relative to that of pristine Cu_2GeSe_3.

To elucidate the origin of the increase in the Seebeck coefficient, the Seebeck coefficient as a function of the carrier concentration (Pisarenko curve) at 300 K is shown in Fig. 4a. The single parabolic band (SPB) model was employed to plot the figure, with further details provided in the Supporting Information[33]. As shown in Fig. 4a, Sn alloying leads to a conspicuous increase in m^* from 1.91 m_e to 2.27 m_e. The increase in m^* enhances the Seebeck coefficient, and the increase in m^* is thought to arise from the greater difference in electronegativity of Sn[34]. Complementary Hall measurements (300–673 K) provide further insight into electrical transport properties. Hall effect measurements reveal a positive Hall coefficient (R_H), which is indicative of p-type conduction of $Cu_2Ge_{1-x}Sn_xSe_3$ (Fig. S5). These findings are mutually consistent with the results of the Seebeck coefficient measurements. As shown in Fig. 4b, n_H decreases monotonically with increasing Sn content (x = 0–0.4) at room temperature, explaining the corresponding reduction in electrical conductivity. The carrier concentrations of the pristine Cu_2GeSe_3 and Cu_2SnSe_3 samples are consistent with those in previous reports, validating our experimental results[17,20]. In contrast to the carrier concentration behavior, the Hall mobility has a nonmonotonic relationship with the Sn content. The optimal mobility is observed for $Cu_2Ge_{0.7}Sn_{0.3}Se_3$, surpassing the values for both the high-alloy $Cu_2Ge_{0.6}Sn_{0.4}Se_3$ and pristine Cu_2SnSe_3 samples. This increase in the mobility of $Cu_2Ge_{0.7}Sn_{0.3}Se_3$ persists despite the higher carrier concentration, indicating a reduction in carrier scattering. Temperature-dependent Hall measurements (Fig. 4c) reveal minimal thermal variation in the carrier concentration, which is characteristic of degenerate semiconductor behavior. The mobility of all the alloyed samples decreases with increasing temperature, which can be attributed to acoustic phonon scattering, as shown in Fig. 4d[35]. This phenomenon explains the reduction in electrical conductivity with increasing temperature shown in Fig. 2a. At elevated temperatures, the mobility of the alloyed samples converges to similar values, which is ascribed to the dominance of acoustic phonon scattering. Sn alloying significantly enhances the mobility of the material relative to that of the pristine material across the entire temperature range. This improvement also suggests that the scattering mechanisms have been modified. The combination of optimized mobility and enhanced m^* significantly improves the PF of the sample.

To elucidate the distinct effects between the Sn solid solution and other dopants, additional doping experiments were

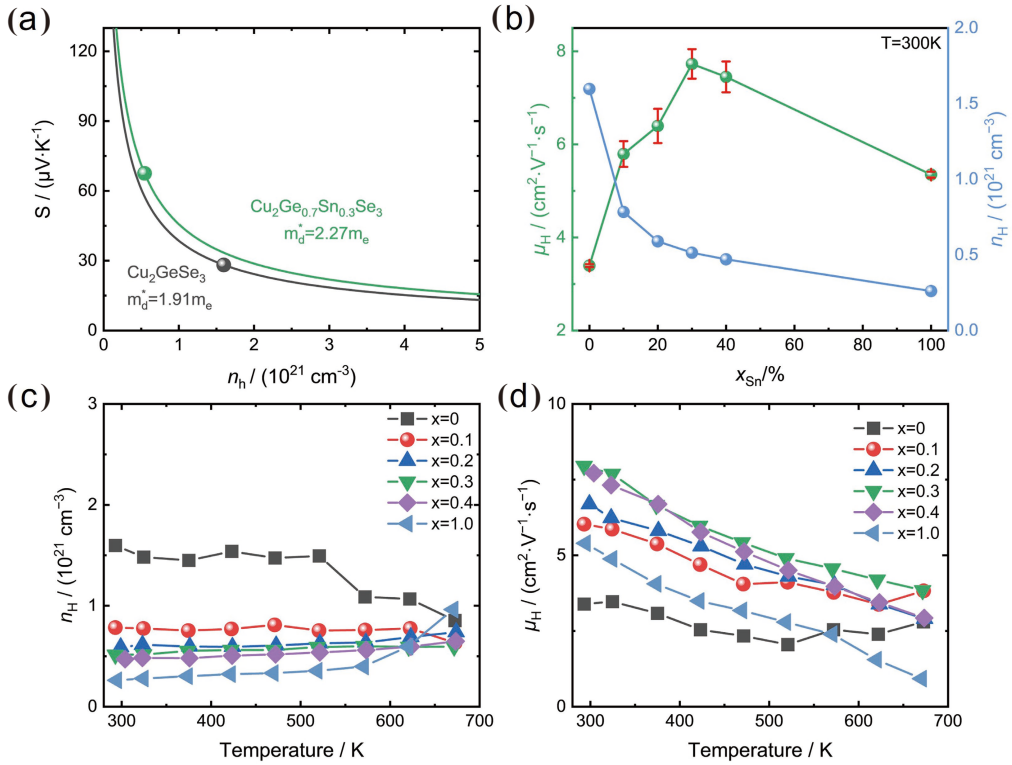


Fig. 4. (a) Pisarenko plot of the Seebeck coefficients as a function of the Hall carrier concentration (n_H) at 300 K. (b) Room temperature Hall concentration (n_H) and Hall mobility (μ_H) of $Cu_2Ge_{1-x}Sn_xSe_3$ ($0 \leq x \leq 0.4$). Temperature-dependent Hall concentration (c) and temperature-dependent Hall mobility (d) of $Cu_2Ge_{1-x}Sn_xSe_3$ ($0 \leq x \leq 0.4$) samples.

CSTR: 32290.14.JUSTC-2025-0118
DOI: 10.52396/JUSTC-2025-0118
JUSTC, **2026**, 56(6):

performed. $Cu_{2-x}Ga_xGeSe_3$, $Cu_{2-x}Zn_xGeSe_3$, $Cu_{2-x}Nb_xGeSe_3$ and $Cu_2GeSe_{3-x}I_x$ samples were prepared, and their electrical properties were measured. The room-temperature carrier concentrations and Hall mobilities for Sn-alloyed and some other doped Cu_2GeSe_3 samples are shown in Fig. 5a (detailed data in Table S3). The Sn-alloyed samples exhibit significantly enhanced mobility relative to that of the other dopants at equivalent carrier concentrations, achieving an ~70% improvement. Owing to this optimized mobility, compared with the other doped counterparts, the Sn-alloyed compounds also achieve a markedly higher peak PF, as clearly demonstrated in Fig. 5b. This improvement in mobility stems fundamentally from modified intrinsic point defects, which critically govern charge transport properties. This computational approach enables direct quantification of how Sn incorporation alters defect formation energies, thereby providing fundamental insights into the observed mobility enhancement. To elucidate the underlying mechanism, we conducted first-principles calculations of the formation energies for the lattice defects in both pristine Cu_2GeSe_3 and $Cu_2Ge_{0.7}Sn_{0.3}Se_3$. The calculated E_{form} for different intrinsic lattice defects in Cu_2GeSe_3 are shown in Fig. 5c. The formation energies in Fig. 5c–e were calculated under the chemical potential conditions of points A, B, and C from Fig. S6, respectively. Compared with the other defects, the V_{Cu} and Cu_{Ge} defects are relatively lower, indicating that the V_{Cu} and Cu_{Ge} defects are the dominant lattice defects in the compound, which is consistent with previous reports[24,26]. The negative values of the defects suggest that V_{Cu} and Cu_{Ge} can spontaneously form during the fabrication process. As shown in Fig. 5c–e, the E_{form} of V_{Cu} and Cu_{Ge} significantly increase after Sn alloying. The increased formation energy suppresses the formation of V_{Cu} and Cu_{Ge} defects. A more purified lattice structure greatly improves the mobility of the material. Moreover, the decrease in the defect concentration leads to a reduction in the hole concentration, which is consistent with the Hall measurement. Thus, Sn incorporation simultaneously optimizes mobility through defect suppression while modulating the carrier concentration, a dual mechanism accounting for the enhanced thermoelectric performance.

To elucidate the thermal transport properties of the $Cu_2Ge_{1-x}Sn_xSe_3$ (x=0–0.4) compounds, the Debye–Callaway model was applied[36–38]. (The relevant parameters and more details are shown in the Supporting Information.) Grain boundary scattering, point defect scattering, and phonon−phonon Umklapp scattering are considered the dominant scattering mechanisms. The spectral lattice thermal conductivity $\kappa(\omega)$ of the $Cu_2Ge_{0.7}Sn_{0.3}Se_3$ sample is shown in Fig. 6a, b. The region between the curves represents the suppression of heat transport attributed to the specific phonon scattering mechanism, providing deeper insights into the reduction in κ_{lat}. Point defect scattering and Umklapp scattering are the main factors affecting thermal conductivity. Point defect scattering has a pronounced influence on phonons with shorter wavelengths, whereas Umklapp scattering is more effective for those with longer wavelengths. Hence, in $Cu_2Ge_{0.7}Sn_{0.3}Se_3$, Sn alloying introduces enhanced point defect scattering, which significantly decreases κ_{lat}. A reduction in κ_{lat} is critical for enhan-

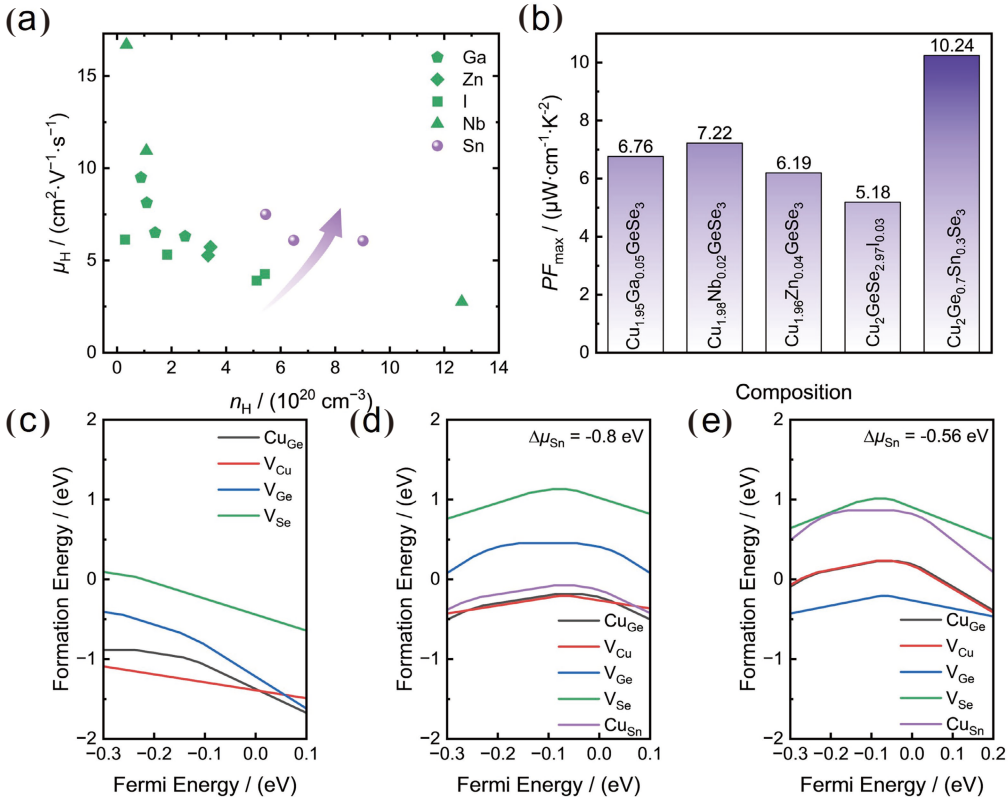


Fig. 5. (a) Comparison of the mobility between Sn-alloyed Cu_2GeSe_3 samples and samples doped with other elements. (b) Peak PF of $Cu_2Ge_{0.7}Sn_{0.3}Se_3$ compared to that of the doped sample. The calculated defect formation energy in Cu_2GeSe_3 as a function of the Fermi level of (c) Cu_2GeSe_3 and $Cu_2Ge_{0.7}Sn_{0.3}Se_3$ with different values of $\Delta\mu_{Sn}$ (d) $\Delta\mu_{Sn} = -0.8$ eV; (e) $\Delta\mu_{Sn} = -0.56$ eV.

CSTR: 32290.14.JUSTC-2025-0118
DOI: 10.52396/JUSTC-2025-0118
JUSTC, **2026**, 56(6):

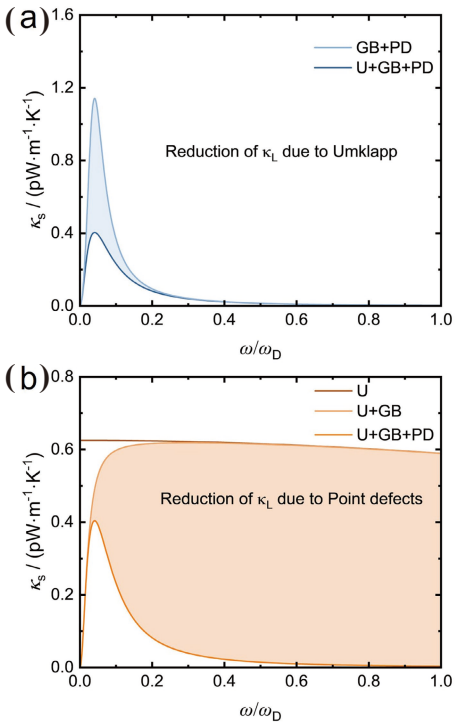


Fig. 6. (a) The reduction in the lattice thermal conductivity caused by Umklapp scattering is marked in blue. (b) The influence of Umklapp scattering on the suppression of lattice thermal conductivity is illustrated in the orange region.

cing the TE performance of materials.

4 Conclusions

In this work, the electrical and thermal transport properties were simultaneously optimized through Sn alloying. The increase in the carrier mobility and decrease in κ_{lat} are responsible for the improvement in the electrical and thermal transport properties, respectively. Moreover, the Seebeck coefficient is dramatically increased because of the larger m^* caused by the greater difference in the electronegativity of Sn. A peak PF value of ~10.22 μW·cm^{-1}·K^{-2} and a κ_{tot} of 1.06·W·m^{-1}·K^{-1} at 723 K are achieved for the $Cu_2Ge_{0.7}Sn_{0.3}Se_3$ sample. Consequently, a peak ZT of 0.66 is achieved at 723 K, which is 130% higher than that of pristine Cu_2GeSe_3. This work demonstrates that alloying is an effective strategy for enhancing thermoelectric performance.

Supporting information

The supporting information for this article can be found online at https:// doi.org/10.52396/JUSTC-2025-0118. The supporting information includes two models, six figures and three tables.

Conflict of interest

The authors declare that they have no conflict of interest.

Acknowledgements

This work was supported by the National Key R&D Program of China (2022YFA1203600), the National Natural Science Foundation of China (T2325021, 22321001, 22109153, 22209167, 22579159), the CAS Project for Young Scientists in Basic Research (YSBR-070), the National Synchrotron Radiation Laboratory Joint Funds of the University of Science and Technology of China (KY2060000241), the Fundamental Research Funds for the Central Universities (WK2490250009, WK9990000166), the Open Foundation of the Anhui Provincial Key Laboratory of Green Carbon Chemistry (FYKFKT24064), and the USTC Bihe Youth Program for Interdisciplinary Innovation (BH-2025XX). The numerical calculations in this paper were performed on the supercomputing system at the Supercomputing Center of the University of Science and Technology of China. This work was partially carried out at the Instruments Center for Physical Science, University of Science and Technology of China.

Biographies

Jiating Xia is a Ph.D. candidate under the supervision of Prof. Chong Xiao in the Hefei National Research Center for Physical Sciences at the Microscale, University of Science and Technology of China. His research focuses primarily on the synthesis and characterization of thermoelectric materials.

Ni Ma is now an Associate Researcher at the State Key Laboratory of Precision and Intelligent Chemistry, USTC. She received her Ph.D. degree from Beijing Normal University in 2020. Her research interests include the syntheses of inorganic solid functional materials and their applications in energy conversion.

References

[1] Bell L E. Cooling, heating, generating power, and recovering waste heat with thermoelectric systems. *Science*, **2008**, *321* (5895): 1457–1461.
[2] Disalvo F J. Thermoelectric cooling and power generation. *Science*, **1999**, *285* (5428): 703–706.
[3] Zhao L D, Dravid V P, Kanatzidis M G. The panoscopic approach to high performance thermoelectrics. *Energy & Environmental Science*, **2014**, *7* (1): 251–268.
[4] Poudel B, Hao Q, Ma Y, et al. High-thermoelectric performance of nanostructured bismuth antimony telluride bulk alloys. *Science*, **2008**, *320* (5876): 634–638.
[5] Biswas K, He J, Blum I D, et al. High-performance bulk thermoelectrics with all-scale hierarchical architectures. *Nature*, **2012**, *489*: 414–418.
[6] Pei Y Z, Shi X Y, LaLonde A, et al. Convergence of electronic bands for high performance bulk thermoelectrics. *Nature*, **2011**, *473*: 66–69.
[7] Luo Z Z, Zhang X, Hua X, et al. High thermoelectric performance in supersaturated solid solutions and nanostructured n‐type PbTe–GeTe. *Advanced Functional Materials*, **2018**, *28* (31): 1801617.
[8] Tan G, Stoumpos C C, Wang S, et al. Subtle roles of Sb and S in regulating the thermoelectric properties of n‐type PbTe to high performance. *Advanced Energy Materials*, **2017**, *7* (18): 1700099.
[9] Heremans J P, Jovovic V, Toberer E S, et al. Enhancement of thermoelectric efficiency in PbTe by distortion of the electronic density of states. *Science*, **2008**, *321* (5888): 554–557.
[10] Zhang Q, Liao B, Lan Y, et al. High thermoelectric performance by resonant dopant indium in nanostructured SnTe. *Proceedings of the National Academy of Sciences of the United States of America*, **2013**, *110* (33): 13261–13266.
[11] Fu C G, Bai S Q, Liu Y T, et al. Realizing high figure of merit in

CSTR: 32290.14.JUSTC-2025-0118
DOI: 10.52396/JUSTC-2025-0118
JUSTC, **2026**, 56(6):

heavy-band p-type half-Heusler thermoelectric materials. *Nature communications*, **2015**, *6*: 8144.
[12] Nielsen M D, Ozolins V, Heremans J P. Lone pair electrons minimize lattice thermal conductivity. *Energy & Environmental Science*, **2013**, *6* (2): 570–578.
[13] Liu H L, Shi X, Xu F F, et al. Copper ion liquid-like thermoelectrics. *Nature Materials*, **2012**, *11*: 422–425.
[14] Plirdpring T, Kurosaki K, Kosuga A, et al. Chalcopyrite $CuGaTe_2$: a high-efficiency bulk thermoelectric material. *Advanced Materials*, **2012**, *24* (27): 3622–3626.
[15] Ishiwata S, Shiomi Y, Lee J S, et al. Extremely high electron mobility in a phonon-glass semimetal. *Nature Materials*, **2013**, *12*: 512–517.
[16] Li Z, Xiao C, Fan S J, et al. Dual vacancies: an effective strategy realizing synergistic optimization of thermoelectric property in BiCuSeO. *Journal of the American Chemical Society*, **2015**, *137* (20): 6587–6593.
[17] Li Y Y, Liu G H, Cao T F, et al. Enhanced thermoelectric properties of Cu_2SnSe_3 by (Ag, In) - co - doping. *Advanced Functional Materials*, **2016**, *26* (33): 6025–6032.
[18] Shi X Y, Xi L L, Fan J, et al. Cu–Se bond network and thermoelectric compounds with complex diamondlike structure. *Chemistry of Materials*, **2010**, *22* (22): 6029–6031.
[19] Rowe D M. CRC handbook of thermoelectrics. Boca Raton: CRC Press, **1995**: 407.
[20] Hu Z Q, Xu H H, Yan C, et al. Enhancement of the thermoelectric performance of Cu_2GeSe_3 via isoelectronic (Ag, S)-co-substitution. *ACS Applied Materials & Interfaces*, **2022**, *14* (18): 20972–20980.
[21] Cho J Y, Shi X, Salvador J R, et al. Thermoelectric properties and investigations of low thermal conductivity in Ga-doped Cu_2GeSe_3. *Physical Review B*, **2011**, *84* (8): 085207.
[22] Wang R F, Li A, Huang T Y, et al. Enhanced thermoelectric performance in Cu_2GeSe_3 via (Ag, Ga)-co-doping on cation sites. *Journal of Alloys and Compounds*, **2018**, *769*: 218–225.
[23] Hu Z Q, Wei R, Yan C, et al. Inducing high power factor in Cu_2GeSe_3-based bulk materials via (Bi, Zn)-co-doping. *ACS Applied Energy Materials*, **2023**, *6* (5): 2962–2972.
[24] Song Q, Qiu P, Chen H, et al. Enhanced carrier mobility and thermoelectric performance in $Cu_2FeSnSe_4$ diamond-like compound via manipulating the intrinsic lattice defects. *Materials Today Physics*, **2018**, *7*: 45–53.
[25] Zhang J X, Zhang Z, Xi L L, et al. Intrinsic defects and the influences on electrical transport properties in quaternary diamond-like compounds: $Cd_2Cu_3In_3Te_8$ as an example. *Journal of Materiomics*, **2022**, *8* (6): 1222–1229.
[26] Zhou Y, Li X, Xi L L, et al. Intrinsic defect study on ternary ABX_2 diamond-like thermoelectric materials and analysis of the density of energy function. *Journal of Materiomics*, **2021**, *7* (1): 19–24.
[27] Liu D R, Wang D Y, Hong T, et al. Lattice plainification advances highly effective SnSe crystalline thermoelectrics. *Science*, **2023**, *380* (6647): 841–846.
[28] Kresse G, Furthmüller J. Efficiency of ab-initio total energy calculations for metals and semiconductors using a plane-wave basis set. *Computational Materials Science*, **1996**, *6* (1): 15–50.
[29] Perdew J P, Burke K, Ernzerhof M. Generalized gradient approximation made simple. *Physical Review Letters*, **1996**, *77* (18): 3865–3868.
[30] Kresse G, Furthmüller J. Efficient iterative schemes for ab initio total-energy calculations using a plane-wave basis set. *Physical Review B*, **1996**, *54* (16): 11169–11186.
[31] Echeverría R, Nieves L, Marcano G. Temperature dependence of the optical properties of manganese - doped Cu_2GeSe_3. *Physica Status Solidi (b)*, **2000**, *220* (1): 285–288.
[32] Kim H S, Gibbs Z M, Tang Y, et al. Characterization of Lorenz number with Seebeck coefficient measurement. *APL Materials*, **2015**, *3* (4): 041506.
[33] Li K, Sun L, Bai W, et al. High-entropy strategy to achieve electronic band convergence for high-performance thermoelectrics. *Journal of the American Chemical Society*, **2024**, *146* (20): 14318–14327.
[34] Zeier W G, Zevalkink A, Gibbs Z M, et al. Thinking like a chemist: intuition in thermoelectric materials. *Angewandte Chemie International Edition*, **2016**, *55* (24): 6826–6841.
[35] Lee Y, Lo S H, Chen C, et al. Contrasting role of antimony and bismuth dopants on the thermoelectric performance of lead selenide. *Nature Communications*, **2014**, *5*: 3640.
[36] Yang G, Niu R, Sang L, et al. Ultra - high thermoelectric performance in bulk BiSbTe/amorphous boron composites with nano - defect architectures. *Advanced Energy Materials*, **2020**, *10* (41): 2000757.
[37] Bai W, Hua Y, Nan P F, et al. Interlayer phonon coupling from heavy and light sublayers in a natural van der Waals superlattice. *Journal of the American Chemical Society*, **2024**, *146* (1): 892–900.
[38] Xie H Y, Su X L, Hao S Q, et al. Large thermal conductivity drops in the diamondoid lattice of $CuFeS_2$ by discordant atom doping. *Journal of the American Chemical Society*, **2019**, *141* (47): 18900–18909.

CSTR: 32290.14.JUSTC-2025-0118
DOI: 10.52396/JUSTC-2025-0118
JUSTC, **2026**, 56(6):